PAPER

NJC
www.rsc.org/njc

Towards novel C–N materials: crystal structures of two polymorphs of guanidinium dicyanamide and their thermal conversion into melamine

Bettina V. Lotsch and Wolfgang Schnick*

Department Chemie und Biochemie, Ludwig-Maximilians-Universität München, Butenandtstraße 5-13 D-81377, München, Germany.
E-mail: wolfgang.schnick@uni-muenchen.de; Fax: +49-89-2180-77440; Tel: +49-89-2180-77436

Received (in Montpellier, France) 11th March 2004, Accepted 25th May 2004
First published as an Advance Article on the web 13th August 2004

Two modifications of the novel guanidinium dicyanamide have been obtained by means of ion-exchange reaction in aqueous or methanolic solution. The hygroscopic compounds were characterized by solution state NMR, mass spectrometry and vibrational spectroscopy. The crystal structures of the polymorphs were elucidated by means of single-crystal X-ray diffraction at 200 K {β-$[C(NH_2)_3][N(CN)_2]$: $Pna2_1$, $Z = 8$, $a = 1373.1(3)$, $b = 495.5(1)$, $c = 1802.9(4)$ pm, $U = 1226.7(4) \times 10^6$ pm^3; α-$[C(NH_2)_3][N(CN)_2]$: $P2_1/c$, $Z = 8$, $a = 1924.9(4)$, $b = 496.0(1)$, $c = 1372.4(3)$ pm, $\beta = 110.46(3)^\circ$, $U = 1227.5(4) \times 10^6$ pm^3} and were found to be largely equivalent in terms of the overall assembly of the molecular ions. Thermodynamic and kinetic aspects of the temperature behaviour of the polymorphs, which is characterized by a succession of thermal events in the temperature region between 240 and 440 K, were assessed by means of temperature-dependent X-ray powder diffraction and thermal analysis. Due to the chemical composition of the novel dicyanamide ($C_3N_6H_6$), which is formally identical with that of melamine $C_3N_3(NH_2)_3$, and its thermal reactivity, which is represented by the facile conversion into melamine around 400 K, guanidinium dicyanamide may be ideally suited as a molecular precursor for chemical approaches toward highly condensed graphitic carbon nitride materials.

DOI: 10.1039/b403788j

Introduction

The ongoing search for the binary carbon nitride C_3N_4 has stimulated various synthetic approaches towards the prototype representative of nitridocarbonates(IV).[1–3] Among the most intensely pursued strategies is the molecular precursor route, based on the principle of building up highly condensed C_xN_y networks *via* condensation reactions of precursors with tailored reactivity.[4–10] To this end, the salts of the dicyanamide anion, $[N{\equiv}C{-}N{-}C{\equiv}N]^-$, have been studied thoroughly as suitable candidates, owing to their pronounced solid-state reactivity leading to a unique variety of thermally induced phase transitions and condensation reactions.

In particular, the alkali salts of dicyanamide trimerize at elevated temperatures, forming the respective alkali salts of the tricyanomelaminate anion.[11–14] Both the product compounds and their partially protonated derivatives, the hydrogentricyanomelaminates,[15,16] are again liable to further thermal condensation due to their side chain electrophilic nitrile carbon atoms. Unlike the alkali dicyanamides, ammonium dicyanamide (NH_4dca) transforms into its molecular isomer dicyandiamide (dda) above 353 K. Upon further heating, dimerization of dda into melamine is observed at temperatures around 443 K.[17,18] The mechanism of the isomerization reaction has been the subject of ongoing studies in our laboratory, representing a model system for a more generalized approach to concepts of solid-state reactivity and the elucidation of reaction mechanisms in the solid phase.[19] On the structural level, the transformation of NH_4dca into dda has been shown to proceed topochemically in the solid state under well-defined reaction conditions. The application of spectroscopic techniques gave evidence of an initial proton transfer from the ammonium cation to a terminal nitrogen atom of the anion, followed by a nucleophilic attack of the *in situ* generated ammonia at the electrophilic nitrile carbon atom.

In order to validate the sketched reaction pathway and to check its transferability to other systems, guanidinium dicyanamide, whose reactivity might well exhibit features similar to its ammonium analogue, has been chosen as a further model system. As yet, the only source of information about the existence of this dicyanamide has been a patent mentioning it as an air-bag component.[20] However, neither structural and spectroscopic data, nor information about the thermal behaviour of guanidinium dicyanamide, is available. Herein we report on the preparation of two modifications of guanidinium dicyanamide by an ion exchange reaction according to Scheme 1. The two polymorphs were characterized by single-crystal X-ray diffraction, variable temperature X-ray powder diffraction, FTIR and Raman as well as solution state NMR spectroscopy, mass spectrometry and thermal analyses.

Results and discussion

Crystal structures

Details of the structure determination and relevant crystallographic data are summarized in Table 1. Interatomic distances and angles are listed in Table 2.†

The orthorhombic unit cell of the β-polymorph ($Pna2_1$, no. 33) contains eight formula units of $[C(NH_2)_3][N(CN)_2]$, of which two build up the asymmetric unit. The guanidinium and dicyanamide ions are alternately stacked and are about

† CCDC reference numbers 240066 and 240067. See http://www.rsc.org/suppdata/nj/b4/b403788j/ for crystallographic data in .cif or other electronic format.

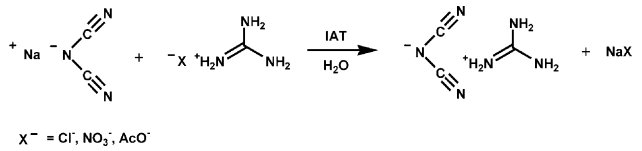

$X^- = Cl^-, NO_3^-, AcO^-$

Scheme 1 Synthesis of guanidinium dicyanamide by means of ion exchange in aqueous solution starting from sodium dicyanamide and a guanidinium salt.

equally spaced, forming arrays of parallel chains along [001] (Fig. 1). The cations of the chains are inclined with respect to [010], their molecular planes being tilted in two different directions while forming angles with the *b* axis of about +40° and −40°, respectively, but being twisted relative to each other. The cations are connected by dicyanamide ions that are arranged in a screw-wise manner along [001] and twisted around their (idealized) C_{2v} axes along [100] (Fig. 2).

The crystal structure of α-$[C(NH_2)_3][N(CN)_2]$ can be described in an analogous way to that of β-$[C(NH_2)_3][N(CN)_2]$. The polymorph crystallizes in the monoclinic space group $P2_1/c$ (no. 14) with lattice constants differing only slightly from those of its orthorhombic counterpart {β-$[C(NH_2)_3][N(CN)_2]$: $a = 1373.1(3)$, $b = 495.5(1)$, $c = 1802.9(4)$ pm, $U = 1226.7(4) \times 10^6$ pm^3; α-$[C(NH_2)_3][N(CN)_2]$: $a = 1924.9(4)$, $b = 496.0(1)$, $c = 1372.4(3)$ pm, $\beta = 110.46(3)°$, $U = 1227.5(4) \times 10^6$ pm^3}.

The molecular ions are stacked alternately along [201] and assembled in an analogous manner as in the orthorhombic form (Fig. 1). The main differences between the two crystal structures, which show variations in the long-range order of the molecules, may become apparent by comparing the spatial orientations of the ions along the equivalent directions: [001] (β) and [201] (α) (Fig. 2). While being tilted with respect to the *b* axis to about the same extent (+40 and −40°) and twisted relative to each other as in the β-form, the planes that are formed about parallel to [001] contain cations with tilt angles alternating in all layers in an AABBA... manner along [201] in the α-polymorph. In the orthorhombic form, the layers are made up alternately by cations with a uniform or with opposite tilt angles. In layers with opposite tilt angles the cations are arranged as ABAB.... along [001]. Thus, although being similar in terms of their principal arrangement, the relative orientation of the anions is different in the two modifications. This corresponds to the differing glide planes in the monoclinic as compared to the orthorhombic space group.

Table 1 Crystallographic data for β-$[C(NH_2)_3][N(CN)_2]$ and α-$[C(NH_2)_3][N(CN)_2]$

	β-$[C(NH_2)_3][N(CN)_2]$	α-$[C(NH_2)_3][N(CN)_2]$
M_w/g mol^{-1}	126.14	126.14
Crystal system	Orthorhombic	Monoclinic
Space group	$Pna2_1$ (no. 33)	$P2_1/c$ (no. 14)
T/K	200	200
a/pm	1373.1(3)	1924.9(4)
b/pm	495.5(1)	496.0(1)
c/pm	1802.9(4)	1372.4(3)
β/°	–	110.46(3)
U/10^6 pm^3	1226.7(4)	1227.5(4)
Z	8	8
ρ_{calcd}/g m^{-3}	1.366	1.365
μ/mm^{-1}	0.102	0.102
Total reflections	16 123	14 135
Indep. reflections	2510	2814
Obs. reflections ($F_o^2 \geq 2\sigma F_o^2$)	1838	1820
R_{int}	0.0499	0.0669
R_1 [$I > 2\sigma(I)$]	0.0423	0.0474
R_1 (all data)	0.0687	0.0860
wR_2 [$I > 2\sigma(I)$]	0.0967[a]	0.1118[b]
wR_2 (all data)	0.1100[a]	0.1290[b]

[a] $w = [\sigma^2(F_o^2) + (0.0569P)^2 + 0.1346P]^{-1}$ where $P = (F_o^2 + 2F_c^2)/3$. [b] $w = [\sigma^2(F_o^2) + (0.0579P)^2 + 0.1554P]^{-1}$ where $P = (F_o^2 + 2F_c^2)/3$.

Table 2 Selected bond lengths (in pm) and angles (in °) for β-$[C(NH_2)_3][N(CN)_2]$ and α-$[C(NH_2)_3][N(CN)_2]$

β-$[C(NH_2)_3][N(CN)_2]$		α-$[C(NH_2)_3][N(CN)_2]$	
C1–N1	131.9(5)	C1–N1	132.6(2)
C1–N3	132.3(3)	C1–N3	132.3(2)
C1–N2	133.7(5)	C1–N2	132.1(2)
C2–N4	133.1(5)	C2–N4	132.5(2)
C2–N5	130.3(5)	C2–N5	132.0(2)
C2–N6	133.2(3)	C2–N6	132.6(2)
C3–N7	115.7(4)	C3–N7	115.2(2)
C3–N8	129.0(4)	C3–N8	128.9(2)
C4–N9	113.1(5)	C4–N9	114.3(2)
C4–N8	132.4(4)	C4–N8	131.0(2)
C5–N10	114.9(4)	C5–N10	115.8(2)
C5–N11	129.5(4)	C5–N11	129.6(2)
C6–N12	115.3(4)	C6–N12	115.0(2)
C6–N11	129.8(4)	C6–N11	130.2(2)
N1–C1–N3	120.8(3)	N1–C1–N3	120.5(2)
N1–C1–N2	119.6(3)	N1–C1–N2	119.7(2)
N2–C1–N3	119.6(3)	N2–C1–N3	119.8(2)
N5–C2–N4	120.7(3)	N5–C2–N4	119.7(2)
N5–C2–N6	119.1(3)	N5–C2–N6	119.6(2)
N4–C2–N6	120.1(3)	N4–C2–N6	120.7(2)
N7–C3–N8	169.8(3)	N7–C3–N8	170.4(2)
N9–C4–N8	174.0(4)	N9–C4–N8	173.6(2)
C3–N8–C4	121.3(3)	C3–N8–C4	122.4(2)
N10–C5–N11	172.4(3)	N10–C5–N11	171.7(2)
N12–C6–N11	174.4(4)	N12–C6–N11	174.3(2)
C5–N11–C6	123.0(2)	C5–N11–C6	121.7(2)

The first coordination spheres of the two crystallographically inequivalent guanidinium ions in β-$[C(NH_2)_3][N(CN)_2]$ and α-$[C(NH_2)_3][N(CN)_2]$ are largely identical with respect to the arrangement of the anions. They are composed of eight dicyanamide ions each, which are grouped in pairs around the central cation with C···N contacts ranging from 325 to 448 pm in both polymorphs (Fig. 3). Of these, six (C2) or five (C1) of the closest anion-cation contacts include terminal nitrogen atoms, whereas the remaining two or three C···N contacts involve bridging amido nitrogens. The three-dimensional hydrogen-bonding network can be characterized in both modifications by the prevalence of medium-strong hydrogen bridges[21] [(N–)H···N 194–260 pm (β) and 204–270 pm (α); angles N–H···N 172–111° (β) and 172–115° (α)].

In a similar way, the two crystallographically inequivalent dicyanamide anions in both polymorphs are surrounded by eight guanidinium ions each, the latter building up two types of layers by the spatial orientation of their molecular planes, which are aligned almost perpendicularly in a 4 + 4 and 6 + 2 manner, respectively (Fig. 4).

The angles (N–C≡N 170–174°, for β and α) and bond lengths [C–N 129–132 pm (β) and 129–131 pm (α), C≡N 113–116 pm (β) and 114–116 pm (α)] of the bent planar dicyanamide anions correspond to the localization of the electron density according to the formula $[N{\equiv}C{-}N{-}C{\equiv}N]^-$, which is in coincidence with the bond lengths observed in other dicyanamides.[11–13,22–24] The planar guanidinium ions exhibit three NCN bond angles that are very close to 120°, and all three C–N bond lengths of the guanidinium cations are essentially equal (Table 2). All three nitrogen atoms are associated with two protons each, corresponding to complete delocalization of the double bond within the C–N backbones and thus, to only minor distortions from D_{3h} point symmetry. The bond lengths and angles of the ions in the monoclinic form show less deviations from the idealized molecular geometries than in the orthorhombic modification.

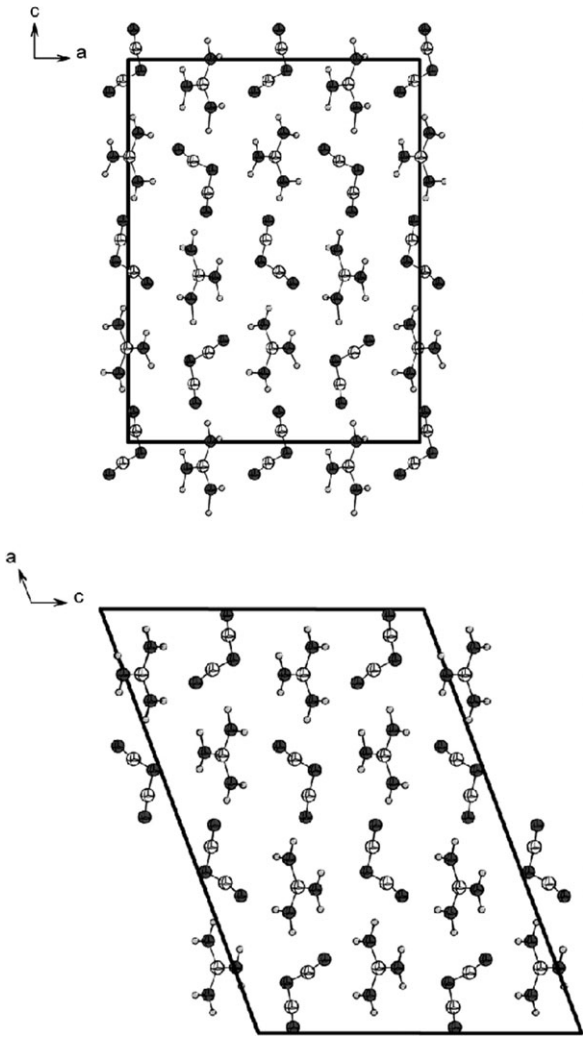

Fig. 1 Crystal structure of (top) β-$[C(NH_2)_3][N(CN)_2]$, view along [010], and (bottom) α-$[C(NH_2)_3][N(CN)_2]$, view along [010]. C: white circles, N: grey circles, H: light grey circles.

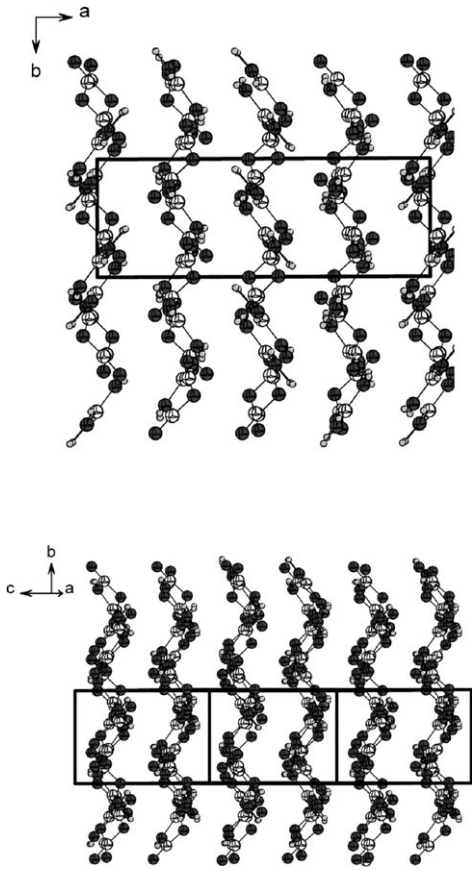

Fig. 2 Crystal structure of (top) β-$[C(NH_2)_3][N(CN)_2]$, view along [001], and (bottom) α-$[C(NH_2)_3][N(CN)_2]$, view along [201]. C: white circles, N: grey circles, H: light grey circles.

The observed X-ray powder data of both modifications could be reproduced and indexed completely by the diffraction patterns calculated on the basis of the respective single-crystal data. Although the energy difference between the two polymorphs at room temperature was found to be extremely small (*cf.* section on thermal behaviour) and, hence, a facile reversible conversion of the two modifications may be expected in the first instance, leading to the coexistence of both phases, the powder patterns obtained were on the contrary almost exclusively of a single phase.

Vibrational spectroscopy

The vibrational spectra of both polymorphs of guanidinium dicyanamide are practically indistinguishable and resemble very much those of other ionic dicyanamides, which are characterized by an intense triplet in the $\nu(C\equiv N)$ region (Figs. 5 and 6).[11,22,24,25]

Raman spectra were recorded *in situ* during the transformation of β- into α-$[C(NH_2)_3][N(CN)_2]$, the differences of the starting material and product spectra, however, being negligibly small. The bands observed in the IR and Raman spectra together with their respective assignments are listed in Table 3.[11,24,26–28] A formal consideration of the theoretical number of vibrations expected for $[C(NH_2)_3][N(CN)_2]$, based on a factor group analysis, requires a total of 264 internal modes after subtraction of the librational and translational lattice modes.[29] However, in a first approximation the internal modes of the molecular ions may be regarded as unaffected by the crystal field due to the weak interionic interactions. Furthermore, the two inequivalent molecules building up the asymmetric unit may not lead to a systematic splitting of the bands if the molecular geometry of the molecules do not differ significantly, thereby reducing the relevant contributions to the internal modes to those from one molecular unit. In total, 3 $N-6$ internal modes per ion ($N=10$ and 5, respectively), giving rise to $24+9=33$ optical modes may be expected. The validity of this simplification is justified by the clarity of the vibrational spectra, in which less than 33 bands are observed.

A splitting of the bands due to the inequivalent sites of the molecules may be disguised by a broadening of the absorptions, which especially applies to the intense bands at 2149 and 1663 cm^{-1} {β-$[C(NH_2)_3][N(CN)_2]$/α-$[C(NH_2)_3][N(CN)_2]$} in the IR spectrum. The IR bands at 1570/1568 and at 1547 cm^{-1} {β-$[C(NH_2)_3][N(CN)_2]$/α-$[C(NH_2)_3][N(CN)_2]$} are associated with the in-plane bending modes of NH_2, the strong absorption at 1653/1663 cm^{-1} is attributed to a coupling of the asymmetric C–N stretching vibration with the in-plane NH_2 bending of the guanidinium ion. These modes, as well as the split bands assigned to the asymmetric and symmetric C–N stretching modes of the dicyanamide ions (Table 3), may be a manifestation of the slightly differing geometry of the two molecules in the asymmetric unit (it should be noted, however, that the absence of the mode at 931 cm^{-1} in the Raman spectrum may invalidate the above assignment).

The differences in the IR spectra of the polymorphs mainly consist in slightly varying band intensities or asymmetries. Besides, minor band shifts are observed that, however, are not exactly reproducible in the Raman spectra. For instance, the high-frequency shift of the N–H stretch at 3450 cm^{-1} for the β-form (α-form 3421 cm^{-1}), as well as the low-frequency shifts of $\nu_{as}(N\equiv C)$ (2141 *vs.* 2149 cm^{-1}) and $\nu_{as}(C–N)+$

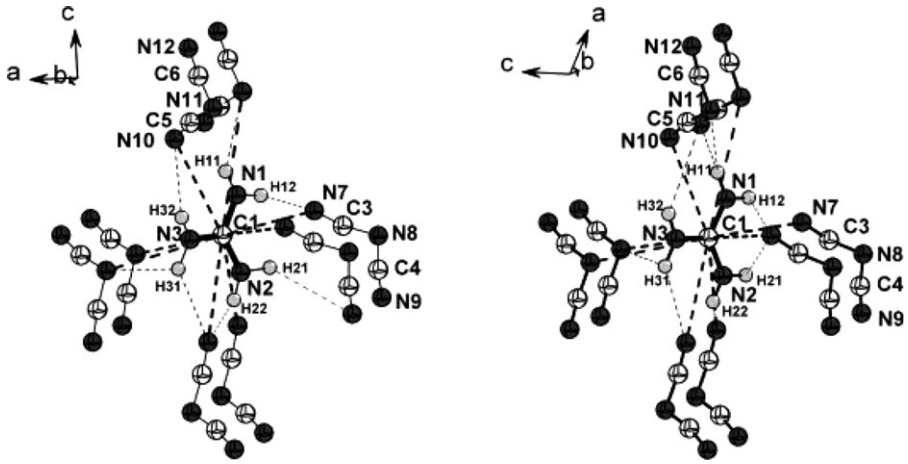

Fig. 3 Coordination sphere of the guanidinium cation I in (left) β-$[C(NH_2)_3][N(CN)_2]$ and (right) α-$[C(NH_2)_3][N(CN)_2]$. The coordination sphere is indicated by dashed lines, hydrogen bonds by dotted lines. C: white circles, N: dark grey circles, H: light grey circles.

$\delta(NH_2)$ (1653 *vs.* 1663 cm^{-1}), may tentatively be associated with the hydrogen bonding network and local geometric differences. The most evident shift associated with the band at 3450 cm^{-1} might be traced back to the less *dense* hydrogen network in the β-form compared to the α-form: whereas in the latter, all H's participate in hydrogen bonding and three H's are involved in a bifurcated hydrogen bond, in the former one hydrogen (H11) does not possess a nearest neighbour acceptor within a sphere of 283 pm and only two bifurcated hydrogen bonds are present. However, comparing the strengths of the *existing* hydrogen bridges in the two modifications, there is evidence for slightly *stronger* bonding in the β-form, which might be substantiated by the red-shift of $\nu_{as}(N\equiv C)$ and the slight blue-shift of $\delta(NH_2)$.

Thermal behaviour

***In situ* X-ray diffractometry.** Variable temperature X-ray powder diffraction measurements have been conducted between 293 and 410 K. When starting from β-$[C(NH_2)_3][N(CN)_2]$, the transformation into α-$[C(NH_2)_3][N(CN)_2]$ can clearly be distinguished at temperatures between 315 and 323 K. Subsequently, melting occurs at 329 K, being followed by a re-solidification around 387 K (Fig. 7). The solidification is accompanied by the emergence of a new phase, which was identified as melamine by X-ray powder diffractometry. When heating α-$[C(NH_2)_3][N(CN)_2]$ from room temperature, no phase transition is observed prior to the melting of the sample (Fig. 7). Comparing the melting points in both temperature runs, minor deviations in the melting onsets become apparent, while the principal temperature characteristics and transformation products are identical for both measurements. Whereas in the case of α-$[C(NH_2)_3][N(CN)_2]$, melting already occurs between 325 and 326 K, β-$[C(NH_2)_3][N(CN)_2]$ does not melt until the transformation into α-$[C(NH_2)_3][N(CN)_2]$ is complete (328–329 K), which effectively delays the melting process slightly.

Differential scanning calorimetry. As a supplement to the temperature-dependent X-ray powder experiments, DSC measurements with samples of both modifications were carried out. The resulting curves (Fig. 8) exhibit two well-distinguishable features between room temperature and 473 K and several weak thermal events in the range 247–293 K. Using a heating ramp of 0.5 K min^{-1}, a sharp endothermic melting signal peaking at 335 K (onset 325 K) is observed for β-$[C(NH_2)_3][N(CN)_2]$, which exhibits a shoulder peak at 332 K prior to the melting signal. This feature, which is not observed when heating the α-form, can be attributed to the phase

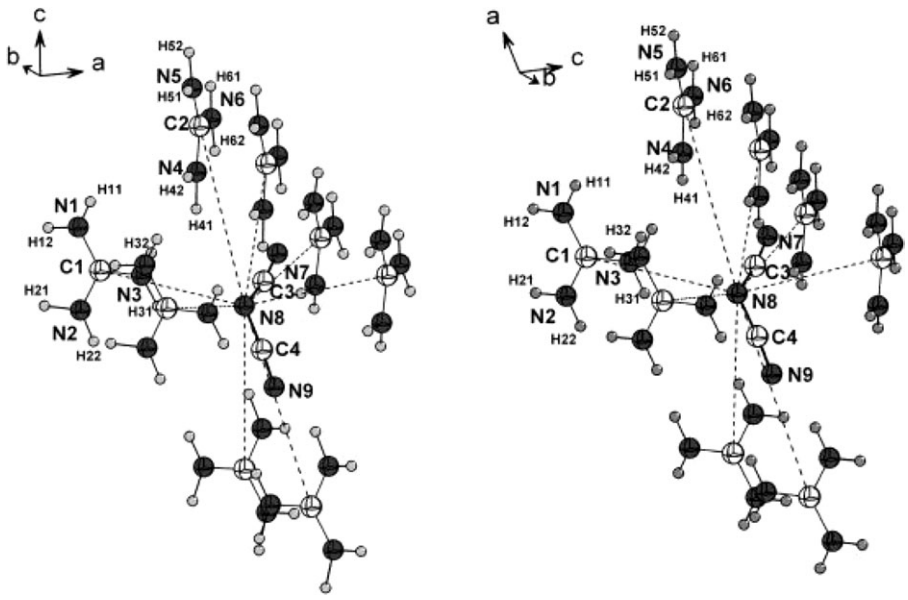

Fig. 4 Coordination sphere of the dicyanamide anion I in (left) β-$[C(NH_2)_3][N(CN)_2]$ and (right) α-$[C(NH_2)_3][N(CN)_2]$. The cations form two types of layers in a 4+4 manner. C: white circles, N: dark grey circles, H: light grey circles.

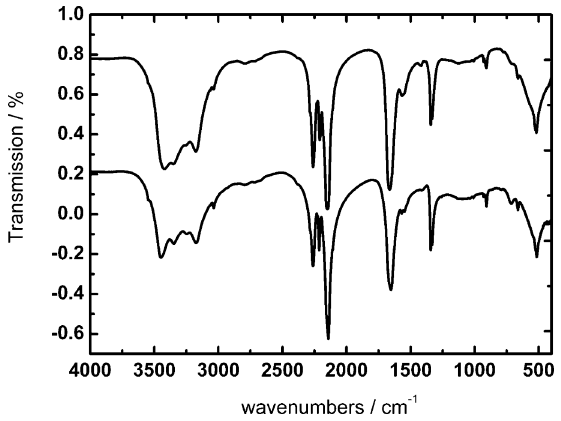

Fig. 5 IR spectra of (bottom) β-$[C(NH_2)_3][N(CN)_2]$ and (top) α-$[C(NH_2)_3][N(CN)_2]$ recorded in the range 4000–400 cm^{-1} at room temperature.

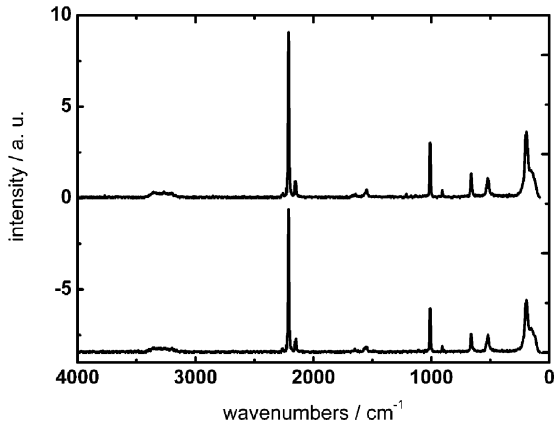

Fig. 6 Raman spectrum of (bottom) β-$[C(NH_2)_3][N(CN)_2]$ and (top) α-$[C(NH_2)_3][N(CN)_2]$ recorded between 4000–80 cm^{-1} at room temperature.

transformation of β- into α-$[C(NH_2)_3][N(CN)_2]$. A strongly exothermic signal with a maximum at 427 K (onset 388 K) can be attributed to the formation of melamine from the melt. Similarly, α-$[C(NH_2)_3][N(CN)_2]$ is melting at 338 K (onset 318 K) and exhibits an exothermic signal at 431 K (onset 395 K). Two more thermal events may be distinguishable at 255 K (endo, β)/254 K (endo, α) and at 293 K (exo, β/endo, α), where for the latter event the sign of energy flow is not clearly distinguishable due to the uneven baseline. The appearance of the cooling curves is strongly dependent on the thermal history of the sample, typically lacking reproducibility of the onset temperatures and appearance of the signals due to the extreme weakness of the thermal events (<0.2 mW). Whereas for β-$[C(NH_2)_3][N(CN)_2]$, weak events are observed at 260 and 252 K (−0.5 K min^{-1}), for α-$[C(NH_2)_3][N(CN)_2]$ three signals (288–285, 262 and 255 K, −0.5 K min^{-1}) are present, which in general are not classifiable unambiguously with respect to the sign of energy flow (Fig. 8). Correlation with the signals obtained from the heating curves is complicated by the variable onsets and large hystereses and was therefore not attempted.

Table 3 Vibrational frequencies (in cm^{-1}) of β-$[C(NH_2)_3][N(CN)_2]$ (upper row) and α-$[C(NH_2)_3][N(CN)_2]$ (lower row) as observed by FTIR and Raman spectroscopies at room temperature. The assignments are based on reference data[a]

IR $\tilde{\nu}_{obs}$	Raman $\tilde{\nu}_{obs}$	Assignment[11,24,26,27]
3449.8, 3348.4, 3245.9 (s, b)	3349, 3199 (w, b)	$\nu_{s/as}(NH_2)$
3421.3, 3347.0, 3175.3 (s, b)	3356, 3268, 3200 (w, b)	
3036.2, 2794.1		comb
3038.2, 2795.0 (w)		
2261.5 (s)	2262 (vw)	$\nu_s(N–C)_{dca} + \nu_{as}(N–C)_{dca}$
2260.5 (s)	2257 (vw)	
2212.7 (ms)	2210 (vs)	$\nu_s(N\equiv C)_{dca}$
2208.9 (ms)	2210 (vs)	
2141.4 (ms)	2148 (ms)	$\nu_{as}(N\equiv C)_{dca}$
2148.7 (vs)	2153 (ms)	
1652.9 (vs)	1650 (vw, b)	$\nu_{as}(C–N)_{gua} + \delta(NH_2)$
1663.4 (vs)	1650 (vw, b)	
1570.0, 1547.1 (ms)	1553 (w, b)	$\delta(N–H_2)$
1567.5, 1547.0 (ms)	1549 (w, b)	
1419.0 (vw)		comb
1417.1 (vw)		
1342.2, 1331.4 (s)		$\nu_{as}(C–N)_{dca}$
1341.4, 1332.2 (s)		
1110.0 (vw, b)	1112 (vw)	$\rho(NH_2)$
1122.8 (vw, b)	1112 (vw)	
1009.6 (vw)	1010 (s)	$\nu_s(C–N)_{gua}$
1007.6 (vw)	1010 (s)	
930.5, 907.7 (w, sh)	907 (w)	$\nu_s(C–N)_{dca}$
930.7, 908.3 (w, sh)	908 (w)	
714.0 (w, b)		$\gamma(CN_3)_{gua} + \omega(NH_2)$
714.0 (w, b))		
662.0 (w, sh)	662 (ms)	$\delta_s(C–N–C)_{dca}$
661.4 (w, sh)	662 (ms)	
545–525 (w,b)		$\gamma_{s/as}(N–C\equiv N)_{dca}$
516.0–523.0 (s)	518 (ms)	$\delta(CN_3)_{gua} + \rho(NH_2)$
518.0–523.0 (s)	523 (ms, b)	$\delta_{as}(N–C\equiv N)_{dca}$
<500 (w)		$\gamma(NH_2)$
<500 (w)		

[a] ν = stretching, δ = in-plane deformation, γ = out-of-plane deformation, ρ = rocking, ω = wagging; vs: very strong, s: strong, ms: medium strong, w: weak, vw: very weak, b: broad, sh: sharp, comb = combination band/overtone.

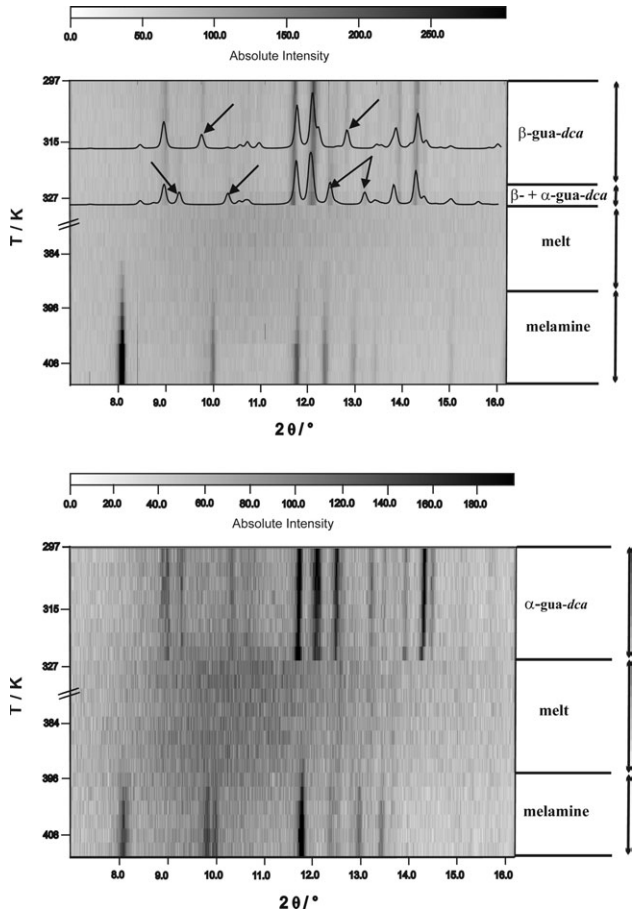

Fig. 7 Variable temperature X-ray powder diffraction patterns of (top) β-$[C(NH_2)_3][N(CN)_2]$ and (bottom) α-$[C(NH_2)_3][N(CN)_2]$ conducted in the temperature range between 297 and 410 K and with a step width of 3 K. The measuring time for each diffractogram (7–16° 2θ) was 20 min and the heating rate for each step 20 K min^{-1}. The β → α phase transition is indicated by arrows.

Complementing these measurements with low-temperature X-ray diffraction at various temperatures between 268 and 200 K reveals that the low-temperature events detected by thermal analyses do not correspond to structural phase transitions, such as the transformation α → β, since the powder patterns of both phases are essentially the same at all temperatures. Therefore, the thermal events below the melting signal observed by DSC may most likely be attributable to phase transitions induced by a change of the reorientational motion of the guanidinium ions. A feature typical for guanidinium salts is the onset of two-dimensional jumps in a three-fold potential around the molecular C_3 axis at sufficiently high temperatures, which may be followed by diffusive rotational motion at higher temperatures. The associated thermal events are observed in a wide temperature range (103–493 K),[6,30–32] largely depending on the anionic sublattice, and are interpreted not only in terms of changes in the rotational state of the cations (order-disorder transitions) but also in the activation energies pertaining to these processes.[31] Therefore, one may assume the thermal anomalies in the low temperature region of both polymers to be associated with order-disorder processes rather than reconstructive phase transitions. To shed light on this issue, spectroscopic approaches such as ^2H solid-state NMR measurements will be necessary. The α → β conversion was not observed to proceed within the measuring interval of typically 2–14 h within the investigated temperature range.

Observations pertaining to the preparation procedures may provide additional information on the relative stability of the two modifications. β-$[C(NH_2)_3][N(CN)_2]$ was only obtained from aqueous solutions that were concentrated under vacuum. Upon storing this polymorph under humid air it deliquesced and subsequently recrystallized as the α-phase. Moreover, samples crystallized as β-$[C(NH_2)_3][N(CN)_2]$ that were stored under atmospheric conditions (regular air humidity) transformed into the α-modification within weeks at room temperature.

The following conclusions may therefore be drawn: β-$[C(NH_2)_3][N(CN)_2]$ is transformed into α-$[C(NH_2)_3][N(CN)_2]$ under atmospheric conditions within weeks and with increased rates upon heating above room temperature. The transformation proceeds endothermically, which may indicate the thermodynamic stability of the β-form at room temperature, while the reverse transformation α → β cannot be effected and, therefore, seems to be kinetically hindered in the temperature range accessible to diffraction experiments. However, since the presence of moisture and/or pressure seems to play a vital role for the conversion of β- into α-$[C(NH_2)_3][N(CN)_2]$ and to promote the transformation even at room temperature, the formation of β-$[C(NH_2)_3][N(CN)_2]$ may require special crystallization conditions. α-$[C(NH_2)_3][N(CN)_2]$ is stable at temperatures around $\geq$ 303 K and, while being metastable, may be super-cooled down to temperatures as low as $\leq$200 K.

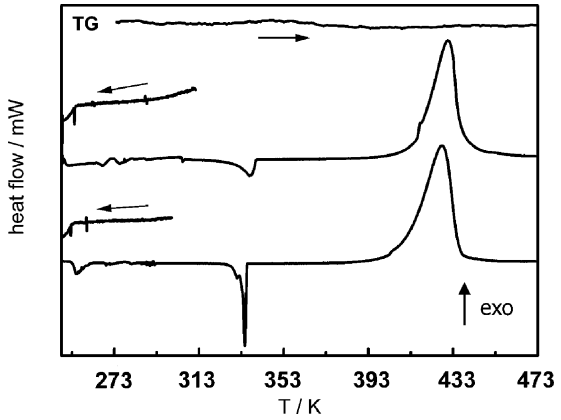

Fig. 8 DSC heating curves and cooling curves of (bottom) β-$[C(NH_2)_3][N(CN)_2]$ and (top) α-$[C(NH_2)_3][N(CN)_2]$ between 247 and 473 K, as well as a TG heating curve of the α-phase, each recorded with a heating (cooling) rate of 0.5 K min^{-1} (the DSC heating curves are normalized and the cooling curves are plotted enlarged). Due to the facile conversion of the β-form into the α-polymorph upon gentle heating, the cooling curves for the β-form were only recorded from 300 K downwards. The endothermic signal of the phase transition β → α prior to the melting onset is clearly distinguishable in the lower curve.

Mechanistic considerations

Regarding the transformation of guanidinium dicyanamide into melamine from the melt reveals an interesting analogy to the thermal behaviour of ammonium dicyanamide. As mentioned above, the latter dicyanamide transforms into dicyandiamide according to the following tentative mechanism, which proceeds in the solid (Scheme 2). Mechanistic aspects of this solid-state transformation were discussed in detail previously.[19]

In case this mechanism is transferable to other solid-state systems, its application to guanidinium dicyanamide results exactly in the observed reactivity (Scheme 3). According to the

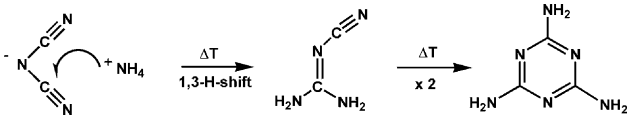

Scheme 2 Mechanism of the solid–solid transformation of ammonium dicyanamide into its molecular isomer dicyandiamide and dimerization of the latter into melamine upon thermal treatment.

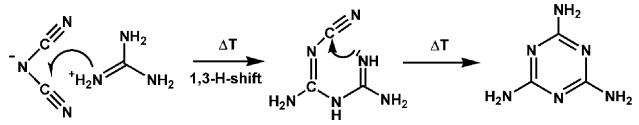

Scheme 3 Mechanism of the transformation of guanidinium dicyanamide into melamine drawn by analogy with the solid-phase reaction of ammonium dicyanamide. A tautomer of cyanobiguanide may be formed as an intermediate.

sketched mechanism, the reaction may be initiated by a proton transfer from the cation to one of the basic centres (terminal N) of the anion, followed by the nucleophilic attack of a guanidinium nitrogen atom at an electrophilic nitrile carbon. As a result, the intermediate formation of a tautomer of cyanobiguanide may occur. Differently from ammonium dicyanamide, the possibility for an intramolecular nucleophilic addition at the remaining nitrile carbon is given, resulting in a ring closure with subsequent formation of melamine.

The observed thermal behaviour of guanidinium dicyanamide may be further strong evidence for the validity of the mechanism proposed for the thermal reactivity of ammonium dicyanamide. It should, however, be noted that since melamine formation proceeds *via* the melt, no identical "solid-state approach" to the reaction pathway is possible and the comparability of the two systems is thus limited. Nevertheless, one may assume the reaction mechanism to operate in an analogous manner as observed for ammonium dicyanamide, yet "solution-like" due to the significantly increased mobility of the molecular ions in the melt.

Conclusion

Two polymorphs of the novel guanidinium dicyanamide have been obtained by means of an ion exchange reaction in aqueous solution. While both modifications are obtained at room temperature, β-$[C(NH_2)_3][N(CN)_2]$ slowly transforms into α-$[C(NH_2)_3][N(CN)_2]$ at temperatures between *ca.* 303–325 K. The crystal structures of the polymorphs (β-form: $Pna2_1$, α-form: $P2_1/c$) are similar, yet not related by a direct group-subgroup relationship. The vibrational spectra of both modifications are essentially identical and can be interpreted by analogy with those of other ionic dicyanamides. The transformation β → α was observed *in situ* by means of temperature-dependent X-ray powder diffraction measurements and by DSC, yet the detection of the reverse transformation failed. After melting, guanidinium dicyanamide recrystallizes as melamine at temperatures around 393 K, which serves as yet another acknowledgement of the thermal reactivity of dicyanamides inferred from previous model studies of ammonium dicyanamide. The established reactivity of guanidinium dicyanamide may be exploited with respect to the design of molecular precursor materials having thermal characteristics suitable for the synthesis of condensed carbon nitride materials.

Experimental

General methods

^1H and ^{13}C NMR spectra were recorded as DMSO-d_6 solutions on a JEOL Eclipse EX-400 instrument, the chemical shifts being referenced with respect to TMS. Mass spectra were obtained using a Jeol MStation JMS-700 gas inlet system. The substances were dissolved in a glycerin-matrix on a copper target and ionized by bombardment with accelerated (6 kV) Xe atoms (FAB^+). Elemental analyses were performed with a C, H, N Elementar Vario EL.

Syntheses

Guanidinium dicyanamide was prepared by an ion exchange reaction in aqueous or methanolic solution. Several guanidinium salts, among which were guanidine hydrochloride $[C(NH_2)_3]Cl$ (Fluka, 98%), guanidine acetate $[C(NH_2)_3]C_2H_3O_2$ (Fluka, 99%) and guanidine nitrate $[C(NH_2)_3]NO_3$ (Fluka, 98%), have been tested as starting materials, yielding similar results. Typically, an aqueous solution of the guanidine salt (1 M), corresponding to 1.5 times the theoretical ion exchange capacity, was poured onto a column containing 20 ml of a strongly acidic ion exchange resin (Merck, Ionenaustauscher I, H^+-Form, Art. 4765). After washing the resin with water (2–3 l), a solution of sodium dicyanamide $Na[N(CN)_2]$ (Fluka, ≥ 96%, 0.5 M, 0.5 times the theoretical exchange capacity) was loaded onto the column. The eluate yielded a strongly hygroscopic white product after evaporation of the water. After re-loading the column with a 1 M HCl solution and cation substitution by means of the respective guanidine salt, the product was purified from residual sodium dicyanamide by dissolving it in a little water and repeating the ion exchange reaction. The aqueous product solution was concentrated at room temperature and the deliquescent product either dried under vacuum or slowly crystallized, using KOH platelets as the water extracting agent. To this end, a bent glass tube filled with KOH and the product, in one part each, was slightly evacuated, yielding a glassy dry product within days, which was stored under argon. It was observed, however, that evaporating the aqueous solution in a beaker open to the atmosphere yielded crystals whose moisture content presumably depends on atmospheric conditions such as temperature and relative humidity.

Crystals of β-$[C(NH_2)_3][N(CN)_2]$ suitable for single-crystal X-ray diffraction were obtained from fresh samples extensively dried under argon and stored at room temperature. Crystals of α-$[C(NH_2)_3][N(CN)_2]$ were obtained from aged crystals contained in moist crystal aggregates and stored open to the atmosphere.

Anal. calcd for $[C(NH_2)_3][N(CN)_2]$: C 28.57, H 4.76, N 66.67%; found: C 28.37, H 4.41, N 64.45% (β); C 29.27, H 5.12, N 64.72% (α). ^1H NMR (400.0 MHz, in DMSO-d_6): δ 6.9 (s, NH_2). ^{13}C {^1H} NMR (100.5 MHz, in DMSO-d_6): δ 119.3 (s, $C{\equiv}N$), 158.4 (s, $C{=}NH_2$). MS (FAB^+): $m/z = 60$ [100%, $C(NH_2)_3^+$].

X-Ray diffraction

X-Ray diffraction data of $[C(NH_2)_3][N(CN)_2]$ single crystals were recorded at 200 K on an ENRAF-NONIUS Kappa CCD four-circle diffractometer equipped with a rotating anode producing graphite monochromated Mo-K_α radiation (λ = 71.073 pm). The crystal structures of both polymorphs were solved by direct methods using the program SHELXTS-97[33] and refined on F^2 applying the full-matrix least-squares method using SHELXTL-97.[34] No absorption correction was carried out due to the weak absorption coefficients of the constituent atoms. The positions of all hydrogen atoms could be determined unequivocally from difference Fourier syntheses and all non-hydrogen atoms were refined anisotropically. Due to the absence of heavy atoms, the Flack parameter of the non-centrosymmetric orthorhombic modification could not be determined.

High temperature *in situ* X-ray diffractometry was performed on a STOE Stadi P powder diffractometer [Ge(111)-monochromated Mo-$K_{\alpha 1}$ radiation, $\lambda = 70.093$ pm] with an integrated furnace using unsealed quartz capillaries. The data collection was restricted to a 2θ range of 7–16° and a single scan collection time of *ca.* 20 min. The sample was heated up to the starting temperature (303 K) by applying a heating rate of 10 K min^{-1} and subsequently in steps of 3 K (heating rate

50 K min^{-1}) to 410 K. Isothermic measurements were conducted at 311, 318, 319 and 321 K in a 2θ range of 8.5–15°, a single scan collection time of 30 min and an initial heating ramp of 5 K min^{-1}.

Low-temperature X-ray powder diffraction measurements at 268, 258, 248, 228 and 200 K were conducted using a STOE Stadi P powder diffractometer [Ge(111)-monochromated Cu–$K_{\alpha 1}$ radiation, $\lambda = 154.060$ pm] equipped with a 600 Series Cryostream Coldhead 707 (Fa. Oxford Cryosystems). The measurements were typically conducted between 10 and 55° 2θ. Between successive measurements starting from ambient temperature, cooling rates of −0.5 or −1 K min^{-1} were applied.

Vibrational spectroscopy

Raman spectra in the range from 80–4000 cm^{-1} were recorded on a Spectrum 2000 NIR-FT-Raman spectrometer (Perkin–Elmer) operating with a Nd-YAG laser optics system ($\lambda = 1064$ mm). During the measurements at ambient temperature, the samples (30 mg) were contained in a sealed glass tube (diameter 2 mm) due to their pronounced deliquescence.

FTIR measurements were carried out on a Bruker IFS 66 v/S spectrometer scanning a range from 400 to 4000 cm^{-1}. The samples were prepared as KBr pellets (5 mg sample, 500 mg KBr) under inert gas conditions in a glove box (β-form) or under atmospheric conditions (α-form).

Thermal analysis

Thermoanalytical measurements were conducted between 247 and 473 K on a Mettler DSC 25 applying a heating rate of 0.5 K min^{-1}. The alumina crucibles used as sample containers were placed in the calorimeter under an atmosphere of dry nitrogen; the cooling was effected by liquid nitrogen or solid carbon dioxide. TG measurements were carried out on a Setaram TG-DTA 92 in Al_2O_3 crucibles under nitrogen between 293 and 573 K using a heating rate of 0.5 K min^{-1}. Additionally, the thermal behaviour of guanidinium dicyanamide was studied by heating samples filled in alumina crucibles, which were contained in glass ampoules, to different temperatures between 473 and 773 K. The products were analyzed by means of powder X-ray diffraction.

Acknowledgements

The authors thank Dipl. Chem. S. Corell and Dr. O. Oeckler for their assistance with the single-crystal X-ray structure elucidation, as well as W. Wünschheim and Dipl. Min. S. Schmid for conducting the DSC/TG measurements. Financial support was granted by the Fonds der Chemischen Industrie and the BMBF (scholarship for B. V. Lotsch) as well as the Deutsche Forschungsgemeinschaft (DFG), which is gratefully acknowledged.

References

1 A. Y. Liu and M. L. Cohen, *Science*, 1989, **245**, 841.
2 C. Niu, Y. Z. Lu and C. M. Lieber, *Science*, 1993, **261**, 334.
3 D. T. Vodak, K. Kim, L. Iordanidis, P. G. Rasmussen, A. J. Matzger and O. M. Yaghi, *Chem.-Eur. J.*, 2003, **9**, 4197.
4 Z. Zhang, K. Leinenweber, M. Bauer, L. A. J. Garvie, P. F. McMillan and G. H. Wolf, *J. Am .Chem. Soc.*, 2001, **123**, 7788.
5 J. Wang and E. G. Gillan, *Thin Solid Films*, 2002, **422**, 62.
6 B. Jürgens, E. Irran, J. Senker, P. Kroll, H. Müller and W. Schnick, *J. Am. Chem. Soc.*, 2003, **125**, 10 288.
7 V. N. Khabashesku, J. L. Zimmermann and J. L. Margrave, *Chem. Mater.*, 2000, **12**, 3264.
8 E. G. Gillan, *Chem. Mater.*, 2000, **12**, 3906.
9 E. Kroke, M. Schwarz, E. Horath-Bordon, P. Kroll, B. Noll and A. D. Norman, *New. J. Chem.*, 2002, **26**, 508.
10 T. J. Komatsu, *J. Mater. Chem.*, 2001, **11**, 802.
11 B. Jürgens, W. Milius, P. Morys and W. Schnick, *Z. Anorg. Allg. Chem.*, 1998, **624**, 91.
12 E. Irran, B. Jürgens and W. Schnick, *Chem.-Eur. J.*, 2001, **7**, 5372.
13 B. Jürgens, E. Irran, J. Schneider and W. Schnick, *Inorg. Chem.*, 2000, **39**, 665.
14 E. Irran, B. Jürgens and W. Schnick, *Solid State Sci.*, 2002, **4**, 1305.
15 B. Jürgens, H. A. Höppe and W. Schnick, *Z. Anorg. Allg. Chem.*, 2004, **630**, 35.
16 B. F. Abrahams, S. J. Egan, B. F. Hoskins and R. Robson, *Chem. Commun.*, 1996, 1099.
17 B. Jürgens, H. A. Höppe, E. Irran and W. Schnick, *Inorg. Chem.*, 2002, **41**, 4849.
18 B. V. Lotsch, J. Senker, W. Kockelmann and W. Schnick, *J. Solid State Chem.*, 2003, **176**, 180.
19 B. V. Lotsch, J. Senker and W. Schnick, *Inorg. Chem.*, 2004, **43**, 895.
20 E. Gast, B. Schmid and P. Semmler, *PCT Int. Appl.*, 1999, WO 9948843 A1 19990930 CAN 131:230642 AN 1999:626150.
21 T. Steiner, *Angew. Chem.*, 2002, **114**, 50; T. Steiner, *Angew. Chem., Int. Ed.*, 2002, **41**, 48.
22 B. Jürgens, E. Irran and W. Schnick, *J. Solid State Chem.*, 2001, **157**, 241.
23 A. P. Purdy, E. House and C. F. George, *Polyhedron*, 1997, **16**, 3671.
24 B. Jürgens, H. A. Höppe and W. Schnick, *Solid State Sci.*, 2002, **4**, 821.
25 M. B. Frankel, E. A. Burns, J. C. Butler and E. R. Wilson, *J. Org. Chem.*, 1963, **28**, 2428.
26 G. Bator, T. Zeegers-Huyskens, R. Jakubas and J. Zaleski, *J. Mol. Struct.*, 2001, **570**, 61.
27 C. L. Angell, N. Sheppard, A. Yamagouchi, T. Shimanouchi and T. Miyazawa, *Trans. Faraday Soc.*, 1957, **53**, 589.
28 M. Szafranski, *Phys. Status Solidi B*, 1997, **201**, 343.
29 D. L. Rousseau, R. P. Baumann and S. P. S. Porto, *J. Raman Spectrosc.*, 1981, **10**, 253.
30 R. Jakubas, P. Ciapala, A. Pietrtaszko, J. Zaleski and J. Kusz, *J. Phys. Chem. Solids*, 1998, **59**, 1309.
31 Y. Furukawa and H. Terao, *Z. Naturforsch., A: Phys. Sci.*, 2002, **57**, 399.
32 M. Yamauchi, S. Ishimaru and R. Ikeda, *Chem. Lett.*, 2003, **32**, 976.
33 G. M. Sheldrick, *SHELXS-97, Program for solution of crystal structures*, University of Göttingen, Germany, 1997.
34 G. M. Sheldrick, *SHELXL-97, Program for refinement of crystal structures*, University of Göttingen, Germany, 1997.